Composites Part B 164 (2019) 158–167

Contents lists available at ScienceDirect

Composites Part B

journal homepage: www.elsevier.com/locate/compositesb

Influence of calcium carbonate on polyamide 12 regarding melting, formability and crystallization properties

Fabio Ippolito[a,c,*], Samuel Rentsch[a], Gunter Hübner[b], Timothy Claypole[c], Patrick Gane[a,d]

[a] Research and Development Department, Omya International AG, Oftringen, CH, Switzerland
[b] Department of Printing and Media, Hochschule der Medien, Stuttgart, DE, Germany
[c] Department of Mechanical Engineering, University of Swansea, Swansea, UK
[d] Department of Bioproducts and Biosystems, Aalto University, Aalto, Helsinki, 00076, Finland

ARTICLE INFO

Keywords:
Smart materials
Thermal properties
Thermal analysis
Sintering

ABSTRACT

Controlling and adjusting the thermal properties of a compound to improve the additive manufacturing process of a polymer matrix through selective laser sintering is of key importance to achieve an optimized final part density as well as hardness. In the past, the purpose of adding mineral fillers to polymers was primarily one of cost reduction. Today, however, fillers are more often used to fulfil a functional role, such as improved thermal or mechanical properties of the polymer composite [1]. In this study, the influence of calcium carbonate as a mineral filler particle on the thermal properties in compression-molded polyamide 12 was investigated. The particle size distribution and the filler amount within the polyamide 12 matrix were varied. The melt viscosity at 190 °C, the melting speed, melting and crystallization point as well as crystallization time at 170 and 172 °C were analyzed. A relationship between these properties and the implementation of a specific amount of calcium carbonate with a certain particle size distribution was observed. The study concludes, that the thermal and flow properties of a polyamide 12 matrix can potentially be manipulated to improve a laser thermal sintering process insofar as the layer melt can be optimized as well as the crystallization process speeded up.

1. Introduction

Additive Manufacturing (AM), also known as 3D printing, is a layer by layer fabrication of 3D objects from a digital model. During the process, material is laid down in individual layers; each layer is bonded/fused together through various techniques (sintering, melting, curing, chemical reactions etc.) [2]. This differs from subtractive manufacturing techniques such as machining that remove material, which is considered a wasteful process in respect to material utilization. AM technologies make it possible to build a large range of functional components with complex geometries which may be difficult, or even impossible, to realize using conventional methods. Furthermore, manufacturing development cycles can be shortened when using AM, thereby reducing production costs [3]. AM technologies have been introduced in various application areas, such as aerospace [4], automotive [5] artistic design [6] and biomedicine [7]. Materials commonly used in AM are often plastic [8] or metals based [9].

In this investigation the focus is on Selective laser sintering (SLS), that uses powder material for the fabrication of different parts directly from computer aided design (CAD) drawings. Various common engineering thermoplastics or metals are used [10]. The most frequently used thermoplastics are polyamides/nylons, typically polyamide 12.

Any polymeric material/composite available in powder form can be processed into a continuum via laser sintering. In practice, however, many factors can prevent a successful processing outcome arising as a result of the materials, most of which can be attributed to the variable thermal behavior properties of the polymer/composite [11].

The optimum particle size of the composite powder, in terms of processability, is generally monodisperse around 45–90 μm displaying high sphericity. However, composites which contain a range of particle sizes, can be of benefit, with the smaller particles filling the gaps between the larger particles to increase density whilst maintaining adequate powder flow [11].

Besides an optimal particle size and morphology of the composite, the chemical interaction between the composite fractions can be of advantage, or disadvantage, as well, influencing both processability (homogeneous distribution and sinterability) as well as final properties. With the correct chemical coating on the additive, chemical interactions between polymer and additive particle can be improved to

* Corresponding author. Research and Development Department, Omya International AG, Oftringen, CH, Switzerland.
E-mail address: fabio.ippolito@omya.com (F. Ippolito).

https://doi.org/10.1016/j.compositesb.2018.11.079
Received 16 July 2018; Received in revised form 18 October 2018; Accepted 15 November 2018
Available online 16 November 2018
1359-8368/

increase processability as well as final properties of the produced element.

During the laser sintering process, the polymer is heated to high temperatures, causing it to change state from a solid to a softer material and then ultimately to a viscous flowing melt. The temperatures at which these transitions occur, and the amount of thermal energy and time required to reach these temperatures, are polymer/composite dependent and have the most significant effect on the ability of the material to be processed successfully by laser sintering [11,12]. The thermal processing window (the temperature range, which leads to a successful sintering process) is narrow. A precise laser power, and exact bed and feed temperatures are required, otherwise the parts could curl or have resulting inhomogeneous density.

For neat polymers, the correct pre-heating temperature and laser energy density is well established. The creation of a new type of composite, however, needs to include an investigation of the thermal properties to find the correct process window. An optimized composite could result in an improved/widened thermal process window with improved, more even thermal transfer and flowability during the process.

2. Methodology

The first step to determine the suitability of a new type of compound for selective laser sintering (SLS) is to compare the thermal and mechanical properties of compression molded compound with those of the virgin polymer. In our case we set out to establish the beneficial role of mineral filler compounded with Polyamide 12 in respect to sintering energy optimization, formability and mechanical properties.

2.1. Materials

The mineral filler used for this study was commonly applied calcium carbonate (GCC), in this case Omyacarb® 10-AV, a marble-derived product provided by Omya International AG (Baslerstrasse 42, 4665 Oftringen, Switzerland).

SLS-approved Polyamide 12 (PA2200) was obtained from EOS e-Manufacturing Solutions (Electro Optical Systems, Robert-Stirling-Ring 1, 82152 Krailling, Germany).

General material specifications are listed in Table 1.

2.2. Pigment production

The various further modifications of the raw filler material were made using a wet grinding process.

The GCC-feed was dispersed in demineralized water to a solids content of 35 wt% and ground in suspension with the use of an agitator ball mill (Dyno®-Mill KDL-Pilot from Willy A. Bachofen AG Maschinenfabrik, 4132 Muttenz, Switzerland) having grinding beads of zirconium dioxide with a particle size of 0.7–1.4 mm.

The volume defined particle size distribution of the resulting suspensions was determined after diluting in demineralized water, stabilizing with approx. 500 ppm of a polyacrylate based dispersant agent, using a laser time-average light scattering particle size analyzer, Malvern Instruments Mastersizer 3000 (Malvern Panalytical Ltd., Enigma Business Park, Grovewood Road, Malvern WR14 1XZ, United Kingdom), adopting the Fraunhofer particle scattering cross-section model.

Table 1
Material specification.

	Omyacarb 10-AV	PA2200
producer/supplier	Omya International	EOS e-Manufacturing
volume-based median particle size	9 µm	60 µm
particle shape	irregular	spherical
approx. thermal conductivity at 298 K	1.3 $W m^{-1}K^{-1}$	0.2 $W m^{-1}K^{-1}$
approx. specific heat	0.8 $kJ kg^{-1}K^{-1}$	1.2 $kJ kg^{-1}K^{-1}$

All ground suspensions were spray dried using a 'GEA Niro MOBILE MINORTM' nozzle spray dryer (GEA Group, Peter-Müller-Strasse 12, 40468 Düsseldorf, Germany) with an atomization temperature of 200 °C, an atomization pressure of 3 bar and an outlet temperature of 90 °C.

The specific surface area (SSA) was determined via nitrogen gas adsorption method (BET-Method) [13] with the use of an ASAP 2460 Surface Area and Porosity Analyzer (Micromeritics®, 4356 Communications Drive, Norcross, GA 30093-2901, USA).

Fig. 1 shows the grinding efficiency of the wet grinding process for the used GCC feed sample. With increasing grinding time, the volume median particle size decreases and the specific surface area of the particles increases. Noteworthy is the observation that although the volume-based median particle size dv_{50}, tends toward a plateau fine value after extended grinding time, the specific surface area continues to rise exponentially. This indicates that the particle size distribution broadens extensively during the grinding process, generating high levels of very fine particles, which, although they do not contribute to a high-volume fraction as dv_{50} tends slowly toward a fine constant, contribute to a rapid increase in the surface area.

Table 2 shows an overview of the resulting properties of the processed filler pigments after the drying step.

2.3. Composite manufacturing

2.3.1. Preparation of formulations

The solid polyamide 12 powder was homogeneously premixed with the specific weight-defined amount of pigment filler, as shown in Table 3. This powder processing resulted in a homogeneously mixed powder blend, which was used directly for compression molding.

Since the interaction between the filler pigment and the polymer occurs at the interface between the two, we choose to describe the surface area introduced by the filler at the given loading per given mass of polymer. Fig. 2 shows an overview of the pigment surface area in ratio to 100 g of polymer in the compound matrix as a function of dv_{50} and increasing filler loading level.

With the chosen filler loading level, we were able to cover the range of up to approx. 150 m^2 of filler material per 100 g of polymer with all given particle size distributions, without influencing the brittleness of the resulting extruded compound. At a filler surface introduction above ~200 m^2 per 100 g polymer, the compound started to lose its elasticity and was, therefore, not included in this study. An increased amount of pigment filler A, higher than 20% weight, was also not included due to a significant increase in the compound melt viscosity resulting from the introduction of such a large amount of coarse pigment filler particles.

2.3.2. Compression molding

Compounds were compression molded via a twin-screw extruder system (Extruder ZE 12 from Three-Tec GmbH, 5703 Seon, Switzerland).

The barrel-length was 25 cm and the twin-screws had a diameter of 12 mm with a flank pitch of 12 mm. The barrel temperature was split in three parts along its length, with an inlet temperature of 160 °C, a compounding zone at 200 °C and an outlet temperature of 170 °C. The twin-screw rotation speed was kept constant for all trials at 90 min^{-1} (rpm), resulting in a compound residence time of approximately 30 s.

The compression molded compound was formed through a filament nozzle with a diameter of 2 mm and granulated into cylindrical pellets with a length ≈1 mm.

The compression molded samples were stored at a constant relative humidity of 50% at a temperature of 22 °C for at least 24 h before analysis.

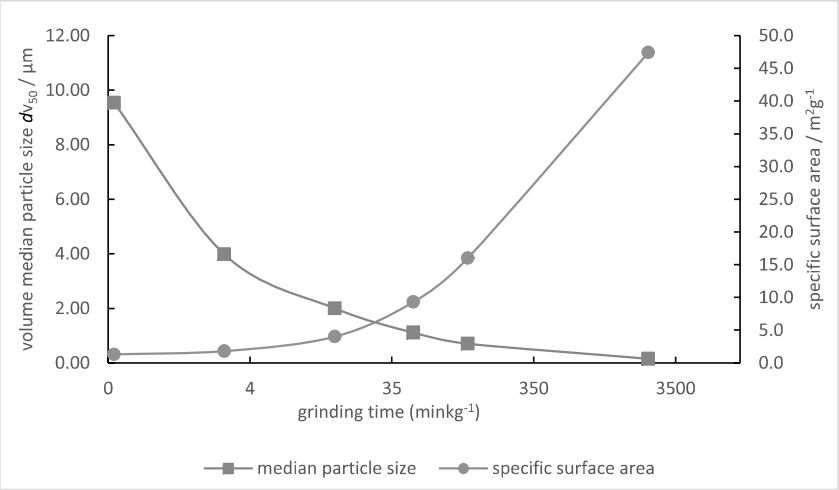

Fig. 1. Wet grinding efficiency of calcium carbonate: comparison of the volume median particle size dv_{50} and the specific surface area in dependency of the grinding time.

Table 2
Resulting pigment data after drying step.

Filler Definition	Grinding time/min.kg^{-1}	dv_{50}/µm	Specific surface area/m^{2}g^{-1}
A	0	10 ± 0.5	1 ± 0.3
B	2	5 ± 0.5	2 ± 0.2
C	14	2 ± 0.1	4 ± 0.5
D	120	1 ± 0.1	16 ± 1.0
E	2250	0.2 ± 0.05	50 ± 3.0

Table 3
Overview of the produced compounds at different filler levels as well as the resulting filler surface in the polymer matrix.

Sample definition	Filler	$CaCO_3$ amount (% weight)	PA2200 amount (% weight)	$CaCO_3$ surface per 100 g PA2200 (m^2)
A.1	**A** dv_{50}:	2.5 ± 0.1	97.5 ± 0.1	**3.3 ± 0.1**
A.2	10 µm	5.0 ± 0.1	95.0 ± 0.1	**6.8 ± 0.5**
A.3	*SSA:*	10.0 ± 0.1	90.0 ± 0.1	**14.4 ± 1.0**
A.4	1 m^2 g^{-1}	20.0 ± 0.1	80.0 ± 0.1	**32.5 ± 2.0**
B.1	**B** dv_{50}:	5.0 ± 0.1	95.0 ± 0.1	**9.5 ± 0.5**
B.2	5 µm	10.0 ± 0.1	90.0 ± 0.1	**20.0 ± 1.0**
B.3	*SSA:*	20.0 ± 0.1	80.0 ± 0.1	**45.0 ± 2.0**
B.4	2 m^2 g^{-1}	40.0 ± 0.1	60.0 ± 0.1	**120.0 ± 5.0**
C.1	**C** dv_{50}:	2.5 ± 0.1	97.5 ± 0.1	**10.3 ± 0.5**
C.2	2 µm	5.0 ± 0.1	95.0 ± 0.1	**21.1 ± 1.0**
C.3	*SSA:*	10.0 ± 0.1	90.0 ± 0.1	**44.4 ± 2.0**
C.4	4 m^2 g^{-1}	20.0 ± 0.1	80.0 ± 0.1	**100.0 ± 5.0**
D.1	**D** dv_{50}:	2.5 ± 0.1	97.5 ± 0.1	**41.0 ± 2.0**
D.2	1 µm	5.0 ± 0.1	95.0 ± 0.1	**84.2 ± 5.0**
D.3	*SSA:*	10.0 ± 0.1	90.0 ± 0.1	**177.8 ± 5.0**
D.4	16 m^2 g^{-1}	20.0 ± 0.1	80.0 ± 0.1	**400.0 ± 10.0**
E.1	**E** dv_{50}:	0.2 ± 0.1	99.8 ± 0.1	**9.0 ± 0.5**
E.2	*0.2* µm	0.5 ± 0.1	99.5 ± 0.1	**24.0 ± 1.0**
E.3	*SSA:*	1.0 ± 0.1	99.0 ± 0.1	**48.0 ± 2.0**
E.4	50 m^2 g^{-1}	2.5 ± 0.1	97.5 ± 0.1	**122.0 ± 5.0**

2.4. Composite analysis

2.4.1. Scanning electron microscopy

The uniformity of compounding, with emphasis on the homogeneity of filler distribution within the polymer/filler matrix, was observed using scanning electron microscopy (SEM).

The granules were pressed above the melting point at a temperature of 210 °C onto a steel metal plate with a thickness of ≈2 mm. The pressed compound samples were embedded in epoxy resin and SEM specimens were prepared by cutting to form a planar internal surface with a diamond knife of 20 µm and afterwards with 15 µm thickness and polishing with corundum (0.05 µm). The specimens were studied with a field emission SEM (Zeiss Sigma VP, Carl-Zeiss-Strasse 22, 73447 Oberkochen, Germany) in variable pressure mode (50 Pa) at 20 kV and a 60 µm cover.

2.4.2. Thermal response analysis

Laser sintering depends on the material heat conductivity, thermal capacity and melt flow properties. Therefore, the phase change behavior in response to the thermal energy input is an important measure of suitability for SLS [14].

2.4.2.1. Melt flow index. The melt flow index (MFI) is defines as the mass flow through a standard die under a given pressure. The units are reported as grams throughput in 10 min, in response to a constant piston pressure at a temperature at/above the melting temperature of the polymer or compound. For a pure polymer the MFI is an assessment of average molecular mass and is an inverse measure of the melt viscosity [14].

The MFI was determined with the use of a CEAST Melt Flow Index Tester Model 702700 (Schenck Technologie-und Industriepark, Landwehrstrasse 65, 64293 Darmstadt, Germany), according to the DIN EN ISO 1133 guidelines.

The compound was pre-heated in the instrument cylindrical barrel for 5 min without pressure load at 190 °C. Afterwards a constant piston pressure, arising from a loading of 2.16 kg, was applied to the material and pressed through a die with a diameter of 2.095 mm. The measuring length, which the material travels in the barrel, was kept constant at 20.00 mm.

2.4.2.2. Thermal mechanical analysis. When polymers in their stationary state are subjected to a high mechanical load (strain), they tend to yield when a critical static stress is reached prior to flow. At its viscoelastic state, the elastic structure may harden as strain increases until the viscous flow dominates after the dynamic yield stress point is reached. Thermal Mechanical Analysis (TMA) provides a technique to study the viscoelastic nature of polymers/compounds at their melting temperature [15,16]. Through TMA analysis the liquefaction rate of a compound can be determined at its melting point as a function of energy input rate, related to the latent heat of the phase change. The thermal melting inflection slope (Tism) shows the percentage force drop occurred at the temperature increase of 1 °C during the melting process of the compound.

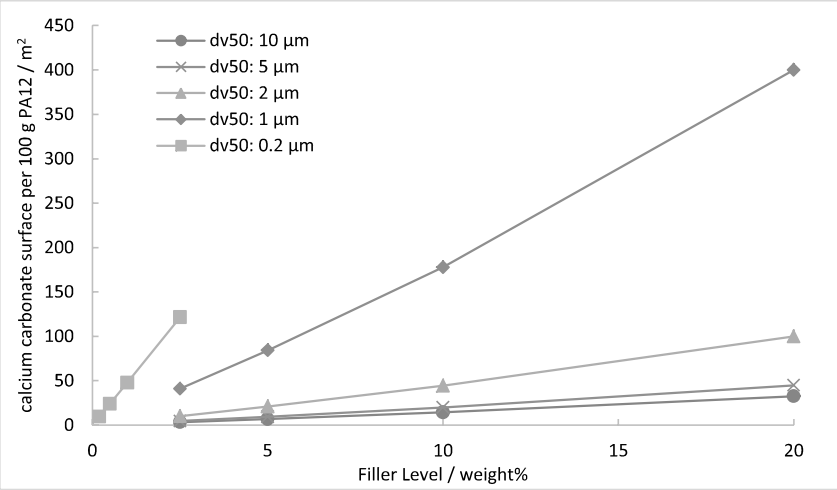

Fig. 2. Resulting pigment surface in the compounded polymer matrix in dependency of the median particle size of the filler material.

A Mettler-Toledo (Im Hackacker 15, 8902 Urdorf, Switzerland) TMA/SDTA 840 apparatus was used to monitor the liquefaction rate of the compounds under a continuous nitrogen flow of 10 $cm^3 min^{-1}$. The samples were heated from 100 °C up to 200 °C at a rate of 10 °C min^{-1} under a constant sample deformation of 0.01 N.

2.4.2.3. Differential scanning calorimetry. The temperature transitions and melting range of polymers and compounds can be observed by recording a difference of the thermal energy response of a sample in relation to a reference material. Differential scanning calorimetry (DSC) records the heat capacity difference as a function of temperature/time. The reference and the sample are heated at a specific heating rate above the melting temperature of the sample, and afterwards cooled at a specific cooling rate under the crystallization point. The differential heat capacity is determined according to whether more or less heat is needed to be given to the sample to maintain both it and the reference at the same temperature [17].

During the melting process, more heat is required to increase the sample temperature at the same rate as the reference. This is due to the absorption of heat by the sample (endothermic phase transition). As the sample crystallizes under cooling, less heat is required to keep the temperature at the reference level due to the exothermic phase transition from liquid to solid.

By observing the difference in heat flow between the sample and reference, differential scanning calorimeters are able to measure the amount of heat absorbed or released during such transitions [18].

DSC curves were recorded on a Mettler-Toledo DSC 823 apparatus under a continuous nitrogen flow of 50 $cm^3 min^{-1}$. The samples (≈7 mg) were heated to 100 °C, kept at constant temperature for 2 min, heated up to 200 °C at a rate of 5 °C min^{-1} and then kept at a constant temperature for an additional 2 min. Afterwards the melt was cooled down to 100 °C at a rate of 5 °C min^{-1} to analyze the exothermic phase transition. Fig. 3 shows the schematic temperature program used for the melting and crystallization temperature determination measurements.

To achieve additional knowledge of the detailed crystallization kinetics, the crystallization time was measured for different constant temperatures to provide a record of the material's isothermal response [19]. The samples (≈7 mg) were heated to 100 °C, kept constant for 2 min, heated up to 200 °C at a rate of 20 °C min^{-1}, cooled down with a cooling rate of 40 °C min^{-1} and finally kept at the measuring temperature of 170 or 172 °C to analyze the crystallization time. Fig. 4 shows the schematic temperature program used for the crystallization time determination measurements.

3. Results and discussion

3.1. Morphology

The SEM pictures in Fig. 5 show the elemental contrast within the sample, where the filler materials reflect more electrons and appear brighter (white spots on the image) than the polymer matrix, which constitutes the black (electron-absorbing) background. The degree of the compounding homogeneity at the relatively high loading level of 20 w/w% filler can be seen across the different SSA values increasing stepwise from 1 $m^2 g^{-1}$ up to 16 $m^2 g^{-1}$. The highest surface area filler (SSA of 50 $m^2 g^{-1}$) is shown only at the low filler level of 2.5%.

It can be seen, as exemplified in the case of sample A with 33 m^2 as well as sample B with 45 m^2 and sample C with 100 m^2 filler per 100 g polymer, the filler material is homogeneously distributed throughout the polymer matrix. There are slight aggregates visible, for the compounds with the higher amount of calcium carbonate with an SSA ≥16 $m^2 g^{-1}$, such as sample D with 400 m^2 or sample E with 122 m^2 of pigment filler per 100 g polymer. Such filler material aggregates, if occurring frequently in the composite, can strongly influence the thermal as well as mechanical properties of the compound. It is well known, that a suitable surface coating of a filler material, like calcium carbonate, in advance of the drying or compounding step, reduces particle-particle interactions, reducing, in turn, the agglomeration behavior. The coating can also be designed to increase the compatibility with the polymer and so additionally improve the dispersing behavior [20]. However, given the relatively homogeneous filler distribution observed in this case, we can conclude that any remaining small agglomerates most likely result from aggregation between the untreated surfaces of the fine particles rather than an inherent incompatibility of the particle surface in contact with the polymer.

3.2. Thermal properties

3.2.1. Melt properties

The determination of the melt viscosity showed a clear dependency on the filler particle size as well as the processing-induced surface in the compound matrix. To express this effect of particle size, independently of surface area, an analysis was made loading to a level that provided equal surface area within the matrix across the various filler samples. As can be seen in Fig. 6, the coarse filler particles show a greater influence on the resulting melt viscosity at 190 °C than the addition of the equivalent surface amount of fine calcium carbonate particles.

Since a quick and homogeneous melt distribution during the laser sintering process is key to efficient and reliable structure forming

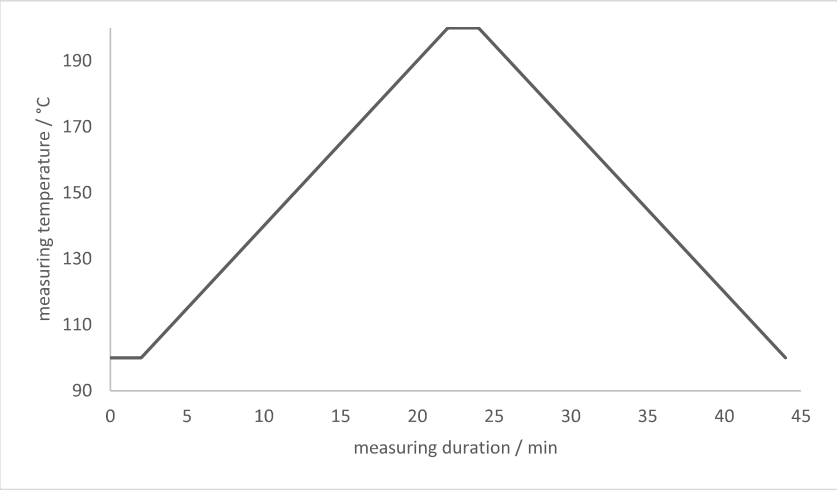

Fig. 3. Schematic temperature program used in differential scanning calorimetry measurements for melting and crystallization behavior.

[11,19], plus sufficient flow and molecular diffusion to intersperse the newly applied layer with the previous one during AM, a large increase of the melt viscosity arising from the addition of filler would not be beneficial. With the use of very fine filler particles in the polymer matrix, the filler material surface-polymer interface can be increased up to 100 m^2 per 100 g Polyamide 12 without influencing the melt viscosity. Using finer filler particles with a smaller single-particle volume than that of coarser filler particles results in a better melt flowability, and hence has less influence on the melt viscosity in comparison with the implementation of coarser calcium carbonate particles.

The determination of the melting speed observed in thermal mechanical analysis indicates that the influence on the melting inflection slope shows a clear filler particle size dependency, as well as filler surface area dependency. Fig. 7 shows how the melting speed can be increased with the implementation of a low amount of larger filler particles in the polymer matrix. With a reduction of the filler particle size, the influence on the melting speed is reduced. A lower Tism-value describes a quicker melting process.

A similar effect can be seen in the DSC determination of the melting point as well as the broadening of the melting transition region. With a low amount of coarser filler particles, the melting point can be lowered, and the transition narrowed significantly, compared with the implementation of finer filler particles. Fig. 8 shows this influence of the particle size as well as filler surface area in the polymer matrix on the melting point and Fig. 9 the additional melting transition breadth behavior, given by the peak width of the total time over which the transition occurs.

We see that finer particles lead to less disturbance of the overall thermal response properties of the polymer, whereas the inclusion of larger particles increases the melt rate and sharpens the transition response, but in doing so raises the melt viscosity. These thermal effects can be explained as resulting from the higher thermal conductivity and lower specific heat of calcium carbonate versus polyamide 12, such that thermal energy is stored less and released more rapidly to the surrounding polymer by the filler particles than the polyamide 12 particles. Due to a higher single-particle volume of the coarser calcium carbonate particles, more thermal energy can be transmitted in comparison with a multitude of single fine filler particles. This results in a greater influence on the melting behavior of the compound with the input of a few coarse instead of many fine calcium carbonate filler particles.

With an increased melting speed and a reduction of the melting

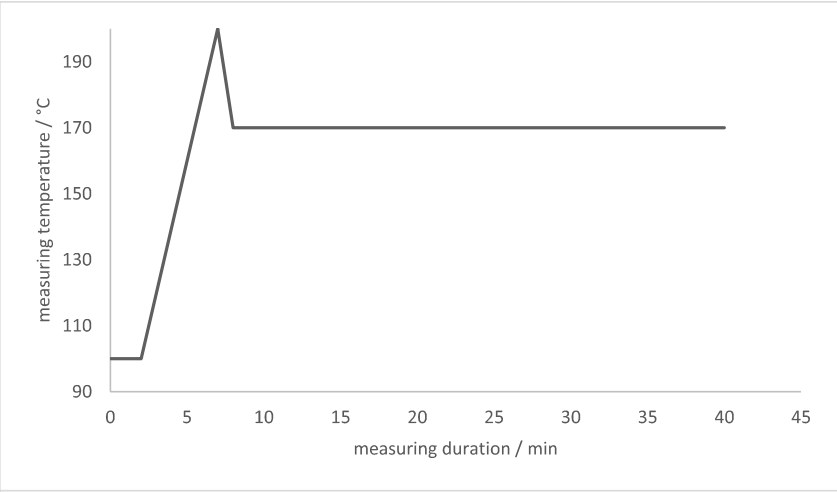

Fig. 4. Schematic temperature program used in differential scanning calorimetry measurements for crystallization time behavior.

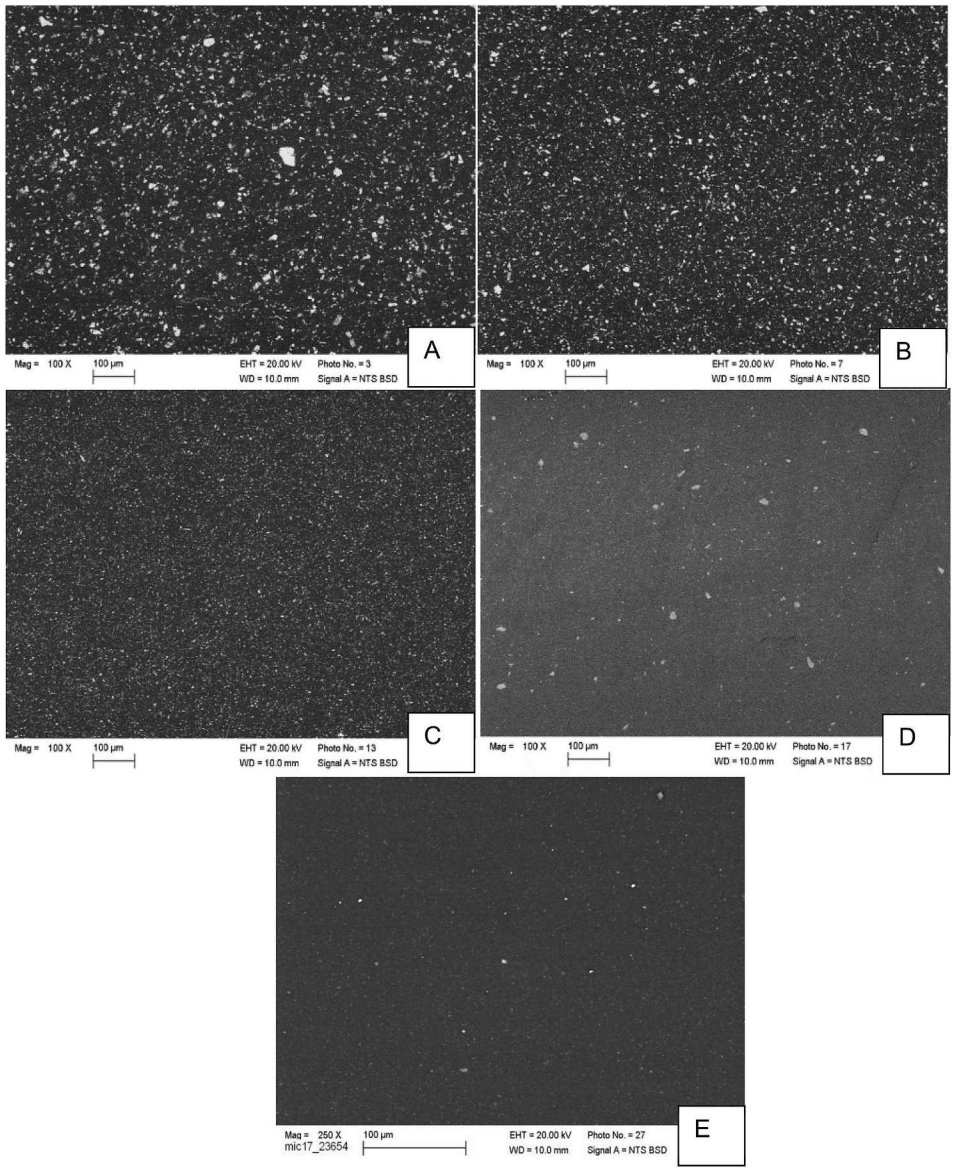

Fig. 5. SEM images of morphology of PA12 – $CaCO_3$ composites; (A) 20 w/w% 1 $m^2 g^{-1}$; (B) 20 w/w% 2 $m^2 g^{-1}$; (C) 20 w/w% 4 $m^2 g^{-1}$; (D) 20 w/w% 16 $m^2 g^{-1}$; (E) 2.5 w/w% 50 $m^2 g^{-1}$

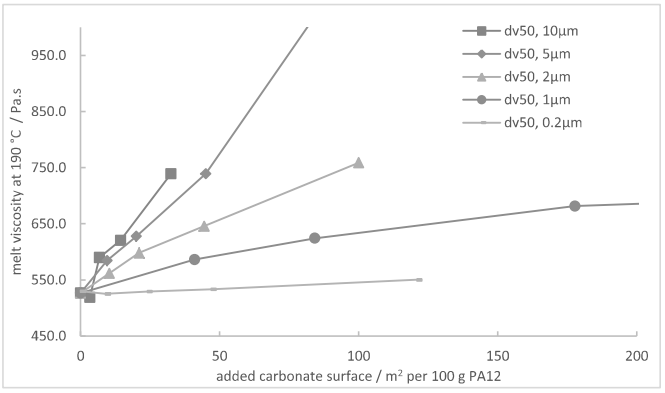

Fig. 6. Melt viscosity at 190 °C against added filler surface in correlation with the volume-based median particle size dv_{50} of the filler material.

point as well as melting transition breadth, the polymer melt can be distributed quicker in the current layer, which is considered to result in an increased final part density as well as a possible increase in printing speed [11].

Fig. 10 reveals the influence of the filler particles on the crystallization point of the polymer compound, detected during cooling in DSC. It can be observed that down to a filler volume median particle size dv_{50} of 1 µm, the influence on the crystallization point shows a clear dependency on added filler surface. With an increased filler surface area in the polymer matrix, independent of the volume median particle size, the crystallization point of the compound can be raised significantly. With the use of sub-micrometer calcium carbonate particles, the influence on the crystallization point can be increased above that of the effect with coarser filler particles. This can be explained with the increased filler particle number in the compound at a given mass loading following the inclusion of submicrometer/nano calcium carbonate particles in the polymer matrix. Due to the reduced single-particle volume of fine filler particles, the amount of nucleation points for a crystallization to occur during the temperature reduction is greater and more homogeneously distributed, resulting in a larger impact on the crystallization point.

With a more detailed analysis of the crystallization kinetics through the determination of the crystallization time at a certain temperature, it

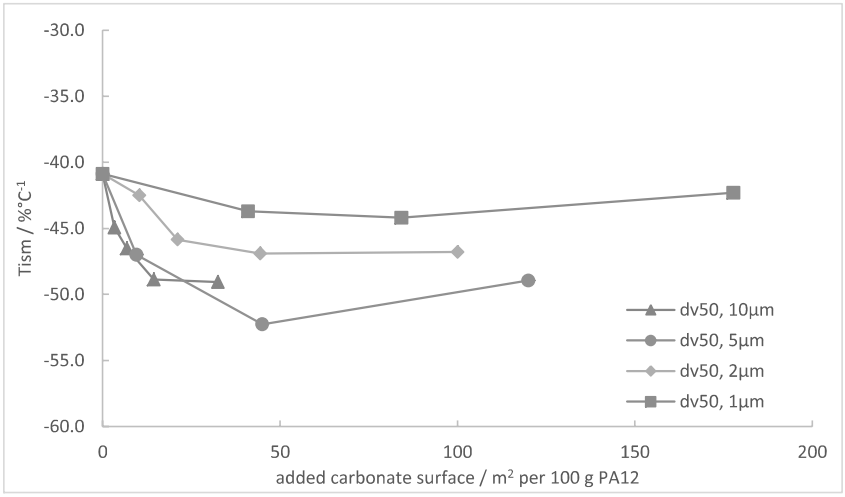

Fig. 7. Thermal Mechanical Analysis - melting inflection slope against added filler surface in correlation with the volume-based median particle size dv_{50} of the filler material.

can be observed that the crystallization kinetics show a clear dependence on the added filler surface area. Fig. 11 shows how the crystallization time on cooling to 170 °C can be manipulated with a given amount of calcium carbonate particles in the polyamide 12 matrix, independent of the volume median particle size of the filler. Thus, the findings clearly support the hypothesis that the crystallization point is dependent on particle number, i.e. nucleation points.

By cooling only to 172 °C, a more precise investigation can be made regarding crystallization time. As a result, it can be observed that a small amount of coarser filler particles has a greater influence on the crystallization time than the equivalent surface area comprising finer particles. In Fig. 12, it can be seen how only a limited amount of $< 20\,m^2$ surface area per 100 g polyamide 12 consisting of coarse filler particles, having a volume-based median particle size $dv_{50} \geq 5\,\mu m$, show a larger reduction of the crystallization time than the equivalent surface area consisting of finer calcium carbonate particles. In the isothermal state of the measurement, the higher single-particle-volume of the coarser filler particles results in the effect that more thermal energy can be taken out of the polymer matrix at a faster rate than with the same amount of associated finer particles. Through this effect, the surrounding polyamide matrix can be cooled down more effectively and, therefore, results in a shorter crystallization time, even though the amount of nucleation points is reduced with the smaller amount of coarser filler particles. Thus, similarly as we saw previously with the melt-comparison, the implementation of finer particles leads to a change in crystallization point, but the use of larger particles reduces the time over which that crystallization occurs.

The speed of the laser sintering additive cycle during part formation is strongly limited by the crystallization time of each layer before the next powder layer can be spread on the previous one. Several different authors have described the influence on the final part density arising from the precise relationship between powder bed temperature, energy density and time between layers [21–26]. It was shown that, if the powder bed temperature is reduced too much, the risk of curling due to rapid cooling rate, and/or shrinking, resulting from a too high laser energy input during the sintering process increases. If the powder bed temperature is set too high, the printing time for each layer will increase and/or the separate layers won't crystallize properly resulting in

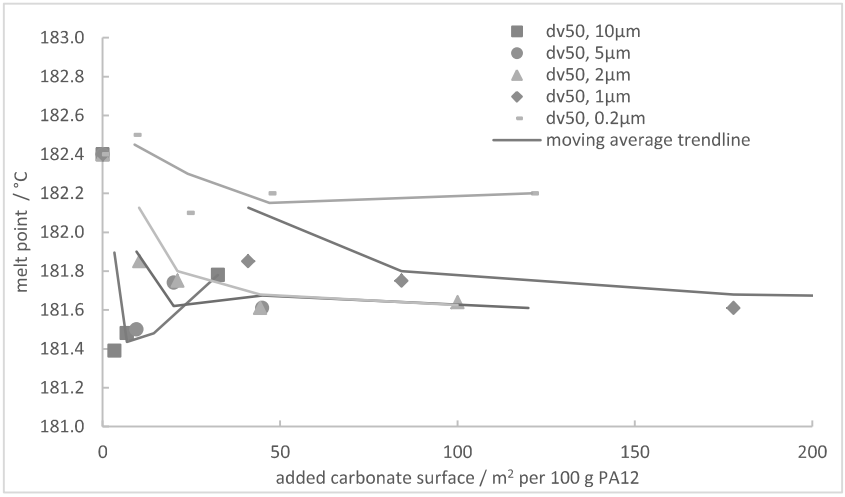

Fig. 8. Differential Scanning Calorimetry – melting point against added filler surface in correlation with the volume-based median particle size dv_{50} of the filler material.

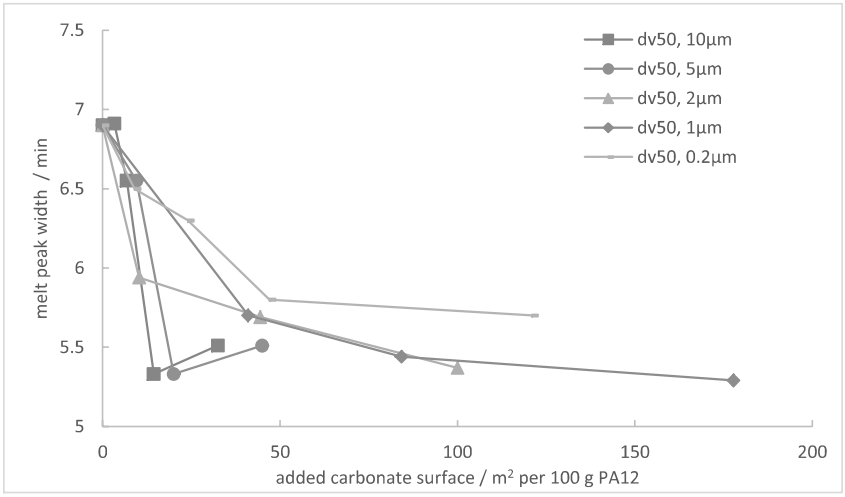

Fig. 9. Differential Scanning Calorimetry – melting peak width as a function of added filler surface in correlation with the volume-based median particle size dv_{50} of the filler material.

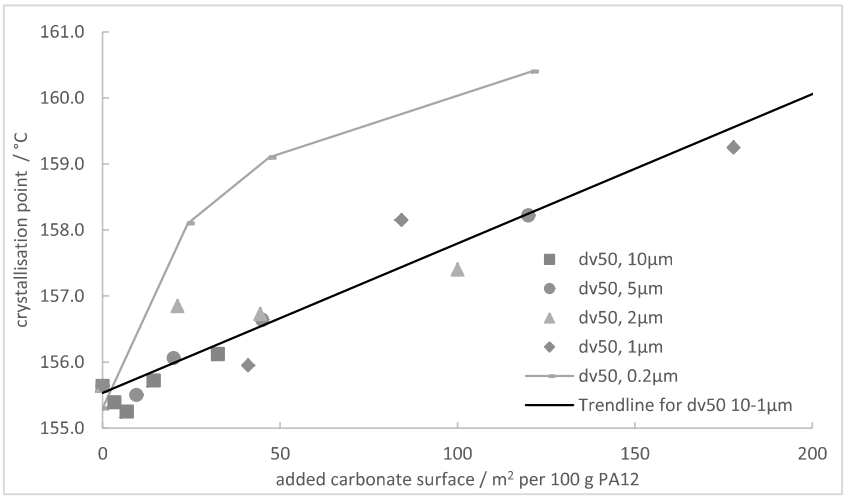

Fig. 10. Differential Scanning Calorimetry – crystallization point as a function of added filler surface in correlation with the volume-based median particle size dv_{50} of the filler material.

a printing failure. With a controlled reduction of the crystallization time for the printing compound, the laser energy input as well as the printing time can be reduced. The well-known property advantages, in respect to material stiffness and controlled impact resistance, on adding calcium carbonate in a polymer matrix can be expected to provide additional resistance to the shrinking/curling behavior [20]. In addition, parts displaying enhanced brightness and opacity can be constructed.

4. Conclusions

In this study, calcium carbonate – polyamide 12 composites have been produced via compression molding using calcium carbonate as filler material with different particle size distribution and related specific surface area. The influence of the filler particle size as well as the added filler surface in the polymer matrix on the thermal properties has been studied with respect to composite sintering and property performance in additive manufacturing processes.

It has been demonstrated that the thermal properties display dependence on the added filler amount as well as the particle size of the filler:

- The melt properties of the compound is highly dependent on the filler volume-based particle size. As finer the calcium carbonate particles in the polymer matrix become, the less influence the filler particles have on the melt:
  - the melting transition shows a particle size as well as filler amount dependency. Coarser calcium carbonate particles generate a marked increase in the rate of melting. With the addition of $\leq 20\ m^2$ of filler surface per 100 g polyamide 12, comprising coarser calcium carbonate particles, the melting speed as well as melt transition width can be significantly reduced.
- The crystallization behavior on cooling shows a particle number and total surface area dependency:
  - with the addition of sub micrometer filler particles, the effect on the crystallization point can be increased markedly. Addition of $\leq 20\ m^2$ of filler surface per 100 g polyamide 12 consisting of coarser calcium carbonate particles, the crystallization time can be significantly reduced. However, adding a high number of fine carbonate particles results in a raising of the crystallization point due to increased nucleation.

In conclusion, the work shows that the thermal and flow properties of a polyamide 12 matrix can potentially be manipulated to improve a thermal sintering process insofar as the layer melt can be optimized as

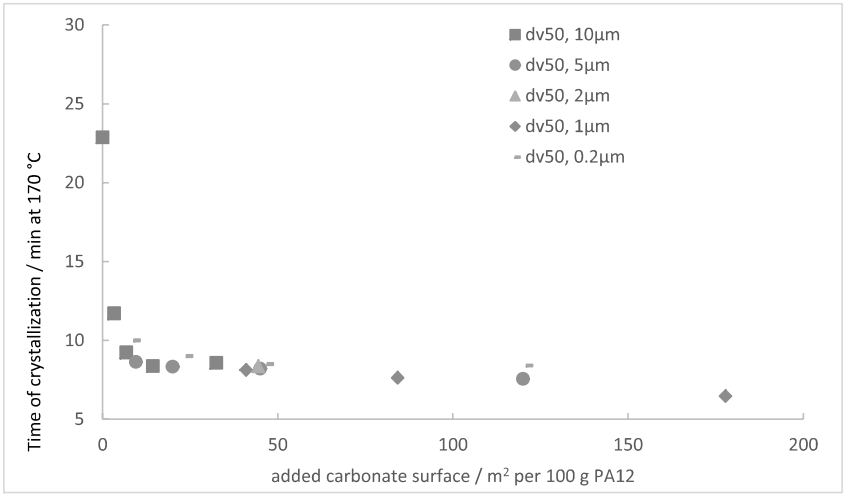

Fig. 11. Differential Scanning Calorimetry - crystallization time at 170 °C against added filler surface in correlation with the volume-based median particle size dv_{50} of the filler material.

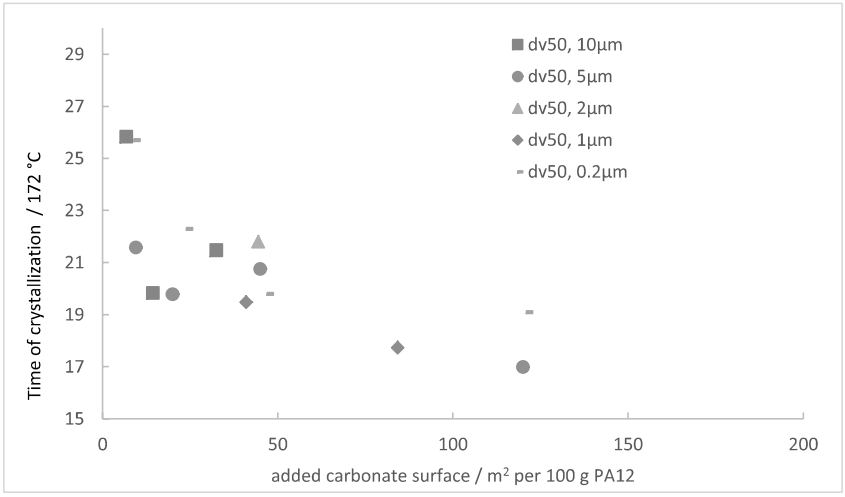

Fig. 12. Differential Scanning Calorimetry - crystallization time at 172 °C against added filler surface in correlation with the volume-based median particle size dv_{50} of the filler material.

well as the crystallization process speeded up.

Further investigations will be conducted on the compound mechanical properties as well as the behavior during the additive manufacturing process.

Acknowledgements

The authors gratefully acknowledge the support and Omya International AG for the financial support as well as providing filler raw material and experimental laboratory facilities.

Appendix A. Supplementary data

Supplementary data to this article can be found online at https://doi.org/10.1016/j.compositesb.2018.11.079.

References

[1] Bartczak Z, Argon AS, Cohen RE, Weinberg M. Toughness mechanism in semi-crystalline polymer blends: II. High-density polyethylene toughened with calcium carbonate filler particles. Polymer 1999;40(9):2347–65.
[2] Mueller B. Additive manufacturing technologies–rapid prototyping to direct digital manufacturing. Assemb Autom 2012;32(2).
[3] Hague R, Mansour S, Saleh N. Design opportunities with rapid manufacturing. Assemb Autom 2003;23(4):346–56.
[4] Rambo CR, Travitzky N, Zimmermann K, Greil P. Synthesis of TiC/Ti–Cu composites by pressureless reactive infiltration of TiCu alloy into carbon preforms fabricated by 3D-printing. Mater Lett 2005;59(8):1028–31.
[5] Murr LE, Gaytan SM, Ceylan A, Martinez E, Martinez JL, Hernandez DH, Machado BI, Ramirez DA, Medina F, Collins S, Wicker RB. Characterization of titanium aluminide alloy components fabricated by additive manufacturing using electron beam melting. Acta Mater 2010;58(5):1887–94.
[6] Petrovic V, Vicente Haro Gonzalez J, Jordá Ferrando O, Delgado Gordillo J, Ramón Blasco Puchades J, Portolés Griñan L. Additive layered manufacturing: sectors of industrial application shown through case studies. Int J Prod Res 2011;49(4):1061–79.
[7] V. Mironov, T. Boland, T. Trusk, G. Forgacs, R.R. Markwald, Organ printing: computer-aided jet-based 3D tissue engineering, Trends Biotechnol 21(4) 157-161.
[8] Hofmann M. 3D printing gets a boost and opportunities with polymer materials. ACS Macro Lett 2014;3(4):382–6.
[9] Gill SS, Kaplas M. Comparative study of 3D printing technologies for rapid casting of aluminium alloy. Mater Manuf Process 2009;24(12):1405–11.
[10] Gibson I, Rosen D, Stucker B. Additive manufacturing technologies: 3D printing, rapid prototyping, and direct digital manufacturing. New York: Springer; 2014.
[11] Goodridge R, Tuck C, Hague R. Laser sintering of polyamides and other polymers. Prog Mater Sci 2012;57(2):229–67.
[12] Rietzel D, Drexler M, Drummer D. Grundlegende Betrachtungen zur Modellierung transienter thermischer Vorgänge beim selektiven Lasersintern von Thermoplasten. RTejournal 2011;8.
[13] Brunauer S, Emmett PH, Teller E. Adsorption of gases in multimolecular layers. J

Am Chem Soc 1938;60(2):309–19.
[14] Kruth J-P, Levy G, Schindel R, Craeghs T, Yasa E. Consolidation of polymer powders by selective laser sintering. Proceedings of the 3rd international conference on polymers and moulds innovations. 2008. p. 15–30.
[15] Zhang Y, Hao L, Savalani M, Harris RA, Tanner K. Characterization and dynamic mechanical analysis of selective laser sintered hydroxyapatite-filled polymeric composites. J Biomed Mater Res 2008;86(3):607–16.
[16] Clark Ligon-Auer S, Schwentenwein M, Gorsche C, Stampfl J, Liska R. Toughening of photo-curable polymer networks: a review. Polym Chem 2016;7(2):257–86.
[17] Höhne GWH, Hemminger W, Flammersheim H-J. Theoretical fundamentals of differential scanning calorimeters, Differential Scanning Calorimetry. Springer; 1996. p. 21–40.
[18] Wunderlich B. Thermal analysis of polymeric materials. Springer Science & Business Media; 2005.
[19] Drummer D, Rietzel D, Kühnlein F. Development of a characterization approach for the sintering behavior of new thermoplastics for selective laser sintering. Physics Procedia 2010;5:533–42. Part B.
[20] Zuiderduin W, Westzaan C, Huetink J, Gaymans R. Toughening of polypropylene with calcium carbonate particles. Polymer 2003;44(1):261–75.
[21] Singh S, Sachdeva A, Sharma VS. Optimization of selective laser sintering process parameters to achieve the maximum density and hardness in polyamide parts. Progress in Additive Manufacturing 2017;2(1):19–30.
[22] Gibson I, Shi D. Material properties and fabrication parameters in selective laser sintering process. Rapid Prototyp J 1997;3(4):129–36.
[23] Williams JD, Deckard CR. Advances in modeling the effects of selected parameters on the SLS process. Rapid Prototyp J 1998;4(2):90–100.
[24] Ho H, Gibson I, Cheung W. Effects of energy density on morphology and properties of selective laser sintered polycarbonate. J Mater Process Technol 1999;89:204–10.
[25] Tontowi AE, Childs T. Density prediction of crystalline polymer sintered parts at various powder bed temperatures. Rapid Prototyp J 2001;7(3):180–4.
[26] Shi Y, Li Z, Sun H, Huang S, Zeng F. Effect of the properties of the polymer materials on the quality of selective laser sintering parts. Proc IME J Mater Des Appl 2004;218(3):247–52.